Kinetic Study of the OH + Isoprene and OH + Ethylene Reactions between 2 and 6 Torr and over the Temperature Range 300−423 K

Bao Chuong and Philip S. Stevens*

School of Public and Environmental Affairs, Indiana University, Bloomington, Indiana 47405

Received: October 11, 1999; In Final Form: March 21, 2000

The rate constants for the OH + isoprene and OH + ethylene reactions have been measured in He with 10% O_2 ($P = 2-6$ Torr) and over the temperature range 300−423 K using a discharge-flow system coupled with laser-induced fluorescence. The measured rate constants for the OH + ethylene reaction are in good agreement with previously reported values. The termolecular rate constant (k_0) at the low-pressure limit for the OH + ethylene reaction was determined to be $(2.62 \pm 0.25) \times 10^{-29}$ cm^6 molecule^{-2} s^{-1} at 300 K where the uncertainty represents 2 standard errors. An Arrhenius expression of $k_0 = (4.9 \pm 0.2) \times 10^{-31} \exp[(1210 \pm 130)/T]$ cm^6 molecule^{-2} s^{-1} was obtained from a weighted linear least-squares fit of the k_0 data versus temperature. The observed negative activation energy ($-E_a/R$) is larger than the currently recommended value. Unlike the OH + ethylene reaction, the rate constant for the OH + isoprene reaction is independent of pressure between 2 and 6 Torr at 300 K. The measured rate constant of $(1.10 \pm 0.04) \times 10^{-10}$ cm^3 molecule^{-1} s^{-1} at 300 K and 2 Torr agrees well with those measured at higher pressures. However, the rate constant for the OH + isoprene reaction begins to show a pressure dependence at temperatures of 343 K and higher. At 343 K, the termolecular rate constant was observed to be $(10.50 \pm 1.57) \times 10^{-27}$ cm^6 molecule^{-2} s^{-1}. An Arrhenius expression of $k_0 = (9.3 \pm 5.4) \times 10^{-29} \exp[(1560 \pm 230)/T]$ cm^6 molecule^{-2} s^{-1} was obtained from a weighted linear least-squares fit of the k_0 data versus temperature. The negative activation energy for the OH + isoprene reaction is similar to that observed for the OH + ethylene reaction.

Introduction

The oxidation of nonmethane hydrocarbons in the troposphere can lead to a significant production of ozone, organic nitrates such as PAN (peroxy acetyl nitrate), and carbonyl compounds.[1,2] Isoprene (2-methyl-1,3-butadiene) and ethylene are two of the more abundant nonmethane hydrocarbons emitted into the atmosphere. In fact, isoprene is the dominant biogenic hydrocarbon emitted by deciduous trees and various other types of vegetation. It is believed that isoprene emissions may be more significant than anthropogenic nonmethane hydrocarbon emissions on regional and global scales due to the relatively large source strength.[3] Because of its high reactivity with the hydroxyl radical (OH), isoprene plays an important role in the photochemistry of urban and rural areas.[4−7] Sources of ethylene include natural (e.g., vegetation, soils, and oceans) and anthropogenic (e.g., biomass burning and fossil fuel consumption) emissions.[2] With an emission rate of 18−45 Tg/yr,[8,9] ethylene can also have a significant impact on photochemical air pollution.

It is generally accepted that at low temperatures (<750 K), OH adds to the double bond of ethylene:[10]

$$OH + C_2H_4 + M \rightarrow HOCH_2CH_2 + M \quad (1)$$

Under atmospheric conditions, O_2 quickly adds to the hydroxyethyl radical to form a β-hydroxyalkyl peroxy radical:

$$HOCH_2CH_2 + O_2 + M \rightarrow HOCH_2CH_2O_2 + M \quad (2)$$

The β-hydroxyalkyl peroxy radical can react with RO_2 and hydroperoxy (HO_2) radicals to form various products. However, under high NO conditions, reaction of the β-hydroxyalkyl peroxy radical with NO forms NO_2, HO_2, aldehydes, and a variety of radical species (reactions 3−5 for example):

$$HOCH_2CH_2O_2 + NO \rightarrow HOCH_2CH_2O + NO_2 \quad (3)$$

$$HOCH_2CH_2O + O_2 \rightarrow HOCH_2CHO + HO_2 \quad (4a)$$

$$HOCH_2CH_2O \rightarrow CH_2O + CH_2OH \quad (4b)$$

$$CH_2OH + O_2 \rightarrow CH_2O + HO_2 \quad (4c)$$

$$HO_2 + NO \rightarrow OH + NO_2 \quad (5)$$

The formation of NO_2 in reactions 3 and 5 can lead to ozone production:

$$NO_2 + h\nu \rightarrow NO + O \quad (6)$$

$$O + O_2 + M \rightarrow O_3 + M \quad (7)$$

There have been several measurements of the rate constant for reaction 1. However, there are discrepancies in the high-pressure-limiting rate constant and the Arrhenius parameters.[11] Also, there are discrepancies in the few measurements of the rate constant at low pressures.[10] Reported measurements of the rate constant for reaction 1 at high pressures using various methods have led to a recommended bimolecular rate constant at the high-pressure limit, k_∞, of 8.52×10^{-12} cm^3 molecule^{-1} s^{-1} at 298 K.[12] The recommended Arrhenius expression for the same reaction at high pressure is $k_\infty = 1.96 \times 10^{-12} \exp(438/T)$ cm^3 molecule^{-1} s^{-1}.[12]

* Corresponding author (E-mail: pstevens@indiana.edu; Fax: (812) 855-7802).

10.1021/jp993613a CCC: $19.00
Published on Web 05/11/2000

As in the case with the OH + ethylene reaction, OH adds to a carbon−carbon double bond in isoprene with the location of addition occurring at four different positions. Addition of OH to the 1 and 4 positions leads to the formation of hydroxy alkyl radicals with resonance character. As a result, each of these radicals leads to the formation of two peroxy radicals after reaction with O_2. Thus, a total of six primary hydroxylalkyl peroxy radicals (RO_2) are formed.[6,7] These peroxy radicals react with NO to form HO_2, NO_2, and a variety of species, such as formaldehyde, methyl vinyl ketone, methacrolein, 3-methylfuran, and other carbonyl compounds (reactions 8−11 for example):[1]

$$OH + CH_2=C(CH_3)CH=CH_2 + M \rightarrow HOCH_2C(CH_3)CH=CH_2 + M \quad (8)$$

$$HOCH_2C(CH_3)CH=CH_2 + O_2 + M \rightarrow HOCH_2C(O_2)(CH_3)CH=CH_2 + M \quad (9)$$

$$HOCH_2C(O_2)(CH_3)CH=CH_2 + NO \rightarrow HOCH_2C(O)(CH_3)CH=CH_2 + NO_2 \quad (10)$$

$$HOCH_2C(O)(CH_3)CH=CH_2 \rightarrow CH_2OH + CH_3C(O)CH=CH_2 \quad (11a)$$

$$CH_2OH + O_2 \rightarrow HCHO + HO_2 \quad (11b)$$

The oxidation of NO to NO_2 leads to ozone production through reactions 5−7.

There have been several measurements of the rate constant of reaction 8.[13−16] Most of these measurements involve relative rate studies in environmental chambers. Very few direct measurements of the rate constant of reaction 8 have been reported, and there have not been any reported measurements of this reaction at pressures <50 Torr. These measurements have led to a recommended value of 1.01×10^{-10} cm^3 molecule^{-1} s^{-1} for the effective bimolecular rate constant for reaction 8 at 300 K and 1 atm, and a recommended Arrhenius expression of 2.54×10^{-11} exp(410/T) cm^3 molecule^{-1} s^{-1}.[12]

However, recent in situ measurements of OH concentrations in the remote troposphere are significantly less than that predicted by current photochemical models,[17] which bring into question the accuracy of our understanding of the chemical sinks of OH in the atmosphere. In addition, measurements of methacrolein and methyl vinyl ketone produced from the oxidation of isoprene were also much lower than predicted, suggesting either a more efficient loss process for these molecules or a less efficient formation process.[17] Clearly, a complete and detailed study of the kinetics of the OH-initiated oxidation of isoprene under a variety of conditions is needed to accurately assess the impact of isoprene oxidation on the concentration of OH and the production of ozone in the troposphere.

This paper presents the results of direct measurements of the rate constant for reactions 1 and 8 with M = He with 10% O_2, at 2−6 Torr, and over the temperature range 300−423 K using the discharge-flow technique. The data for isoprene are the first set of direct measurements for this pressure range.

Experimental Section

The discharge-flow system used in this study is similar to those described in detail elsewhere.[18] Briefly, the system consists of a 66-cm long, 2.5-cm i.d. Pyrex flow reactor that is connected to an aluminum detection chamber. For room-temperature experiments, the reactor was coated with a thin film of halocarbon wax (Halocarbon Corporation) to minimize wall losses of reactive species. At temperatures >300 K, a Teflon tube (2.3-cm i.d.) was inserted into the reactor to replace the halocarbon wax. The flow tube was wrapped with heating tape to heat the reactor for high-temperature experiments. Temperature was monitored with a thermocouple inserted into the region of the flow tube where isoprene is injected. This thermocouple was calibrated against a movable thermocouple probe, the position of which was varied inside the heated area of the flow tube. This calibration did not reveal any temperature gradients in the heated region of the flow tube. The flow system was evacuated by a mechanical pump (Leybold D16B), resulting in a bulk flow velocity of 10.1−14.7 m s^{-1} at 300−423 K. A MKS Baratron capacitance manometer was used to measure the average pressure in the main reaction zone.

All experiments were done under pseudo-first-order kinetic conditions. Concentrations of dilute mixtures of isoprene (Aldrich, 99%) were added in excess through a movable Pyrex injector (6-mm o.d.) coated with halocarbon wax. The concentrations were determined by measuring the pressure drop in a calibrated volume over time. To prepare the mixtures, known aliquots of degassed isoprene were vacuum-distilled into the calibrated volume and diluted with ultrahigh purity (UHP) He (99.999%). For the ethylene experiments, the same movable injector was used, but pure ethylene (99.5%) was used and the concentration was determined from either the flow rate through a flow controller (MKS 1179) or the pressure drop in a calibrated volume over time.

The addition of isoprene and (to a lesser extent) ethylene to the flow system increases the heterogeneous loss of OH on the reactor walls. This result is likely due to reversible adsorption of isoprene onto the walls of the reactor because the OH signal recovered to its initial value slowly after the isoprene was turned off at the end of the decay. This effect has been observed previously in experimental studies of the Cl + isoprene reaction.[19,20] The addition of a small amount of O_2 has been found to inhibit isoprene- and ethylene-catalyzed OH wall reactivity. Unlike experiments in He alone, the OH signal recovers to its initial value quickly in the presence of O_2 after turning off the isoprene flow at the end of a decay.[13] This quick recovery may be due to an inhibition of the isoprene-catalyzed OH wall reactivity by O_2. Although the overall rate constant for the OH + isoprene reaction was not greatly affected by the addition of the small amount of O_2 [$k_{He} = (9.6 \pm 0.5) \times 10^{-11}$ cm^3 molecule^{-1} s^{-1}, $k_{He+O2} = (1.10 \pm 0.05) \times 10^{-10}$ cm^3 molecule^{-1} s^{-1}, 2 Torr and 298 K],[13] the intercept and scatter of the plots of k^I versus isoprene concentration were reduced in the presence of O_2, and thus improved the overall accuracy and precision of the measurement.[13] However, it should be noted that the measurements in 10% O_2 may be influenced by the increased collisional efficiency of O_2 relative to He. The O_2 (∼10% of the bulk flow) was added through a fixed injector 11-cm downstream of the radical source for all experiments.

The OH radicals were produced by the F + $H_2O \rightarrow$ OH + HF reaction. The F radicals were generated by a microwave discharge of a gaseous mixture of CF_4 and He through a fixed injector upstream of the main reaction zone. Concentrations of H_2O (<5×10^{13} cm^{-3}) was added 1.3 cm upstream of the F radical injector by bubbling He through a trap containing distilled H_2O. This source was used instead of the H + $NO_2 \rightarrow$ OH + NO reaction to minimize potential secondary chemistry due to reactions 3 or 10 that could interfere with the rate constant measurements in the presence of O_2. The OH radicals were detected by laser-induced fluorescence (LIF) using the frequency-

TABLE 1: OH + Ethylene Summary of Experimental Conditions and Results

T (K)	[He] (10^{16} molecules cm^{-3})	[Ethylene] (10^{13} molecules cm^{-3})	No. of Expts	k^{II} (10^{-12} cm^3 molecule^{-1} s^{-1})[a]
300	6.44	2.4−13.3	15	1.05 ± 0.03
	12.97	2.9−13.6	15	1.51 ± 0.04
	18.54	3.0−9.5	14	1.97 ± 0.09
343	5.60	2.4−20.6	14	0.70 ± 0.02
	11.06	2.8−17.5	13	1.00 ± 0.02
	16.57	3.2−19.0	13	1.34 ± 0.09
366	5.20	2.9−26.1	13	0.53 ± 0.05
	10.21	3.4−19.3	13	0.77 ± 0.03
	15.56	1.5−21.5	13	0.99 ± 0.05
393	5.16	5.4−25.6	12	0.43 ± 0.02
	9.78	4.9−23.9	12	0.60 ± 0.02
	15.38	2.2−20.4	12	0.79 ± 0.07
423	5.11	5.6−30.2	12	0.37 ± 0.02
	8.72	8.4−29.9	13	0.47 ± 0.03
	14.35	3.1−19.1	13	0.61 ± 0.03

Flow velocity	10.8−14.5 m s^{-1}
Carrier gas	He w/10% O_2
OH concentration	$<3 \times 10^{11}$ cm^{-3}
O_2 concentration	$(2-8) \times 10^{15}$ cm^{-3}
Stoichiometric ratio	∼150−2600
Diffusion coefficient	OH in He, $0.145T^{3/2}/P$ (<5% correction)
First-order wall removal rate	<6 s^{-1} (in presence of 10% O_2)

[a] Uncertainties represent 2 standard errors.

doubled output of a 20 Hz Nd:YAG-pumped dye laser (Lambda Physik). The excitation of the A−X (1,0) band via the $Q_1(1)$ transition near 282 nm resulted in the OH A−X (0,0) fluorescence near 308 nm. This fluorescence passes through a UG-11 color glass filter and a 10-nm band-pass, 20% transmissive interference filter centered at 308 nm (Esco Products) before being detected by a photomultiplier tube equipped with photon-counting electronics (Hamamatsu H5920−01).

To minimize the signal due to laser light scatter and background fluorescence, the detection of the OH fluorescence was electronically gated. The gate was turned on ∼10 ns after the laser pulse, and remained on for ∼300 ns to collect the OH fluorescence. To prevent saturation of the photon-counting electronics and of the OH absorption, the average laser power was kept <0.5 mW. At 0.4 mW, the sensitivity of the detection system was measured to be $\sim 1 \times 10^{-8}$ counts s^{-1} cm^3 molecule^{-1} after calibration using the $H + NO_2 \rightarrow OH + NO$ reaction. For these calibrations, a known amount of NO_2 (measured from the pressure drop in the calibrated volume) was titrated in an excess of H atoms produced from a microwave discharge of trace H_2 in He. With a typical background signal of 50−100 counts s^{-1}, the OH detection limit was determined to be $\sim 3 \times 10^8$ molecules cm^{-3} (S/N = 1, 10-s integration). For these experiments, the typical initial OH concentrations was between 1 and 2×10^{11} cm^{-3}.

Results and Discussion

The pseudo-first-order decay rates (k^I_{obsd}) were obtained from a weighted linear least-squares fit of the logarithm of the detected OH fluorescence signal versus time, as determined from the injector distance for reaction under the plug flow approximation (k^I_{decay}). The k^I_{obsd} values were corrected for axial diffusion and radical loss on the movable injector as follows:[21]

$$k^I_{obsd} = k^I_{decay}\,(1 + k^I_{decay} D/v^2) - k_{probe} \qquad (12)$$

In this equation, D is the radical diffusion coefficient, v is the mean bulk flow velocity, and k_{probe} is the radical loss rate on the movable injector, measured in the absence of ethylene or isoprene. The effective bimolecular rate constants (k^{II}) at various pressures and temperatures were calculated from a weighted linear least-squares fit of k^I_{obsd} versus alkene concentration.

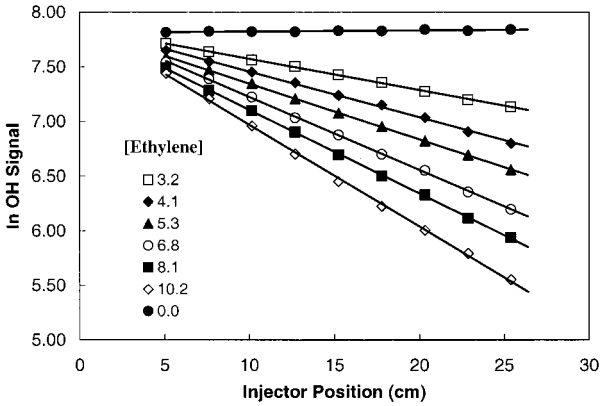

Figure 1. Sample pseudo-first-order decays of OH for the OH + ethylene reaction at 2 Torr and 300 K (ethylene concentrations in 10^{13} cm^{-3}).

OH + Ethylene. The pressure dependence of k^{II} for reaction 1 was studied at five different temperatures in the range 300−423 K. The experimental conditions and the measured rate constants are summarized in Table 1. The reported uncertainties in Table 1 represent two standard errors from the weighted fit.

A series of typical first-order decay plots for reaction 1 is shown in Figure 1 and typical plots of k^I_{obsd} versus ethylene concentration for the data at 2 Torr of He with 10% O_2 and 300, 343, and 423 K appear in Figure 2. A weighted least-squares fit of the 300 K plot yields a value of $k^{II}_{300} = (1.05 \pm 0.03) \times 10^{-12}$ cm^3 molecule^{-1} s^{-1} for the effective bimolecular rate constant at room temperature and 2 Torr of He with 10% O_2. The measured rate constant at 2 Torr of He with 10% O_2 and others at higher pressures and 300 K (as listed in Table 1) are in good agreement with direct measurements reported by Kuo and Lee[10] ($P = 1-5$ Torr He, discharge flow − resonance fluorescence), by Howard[22] ($P = 1-7$ Torr He, discharge flow − laser magnetic resonance), and by Bradley et al.[23] ($P = 2.9$

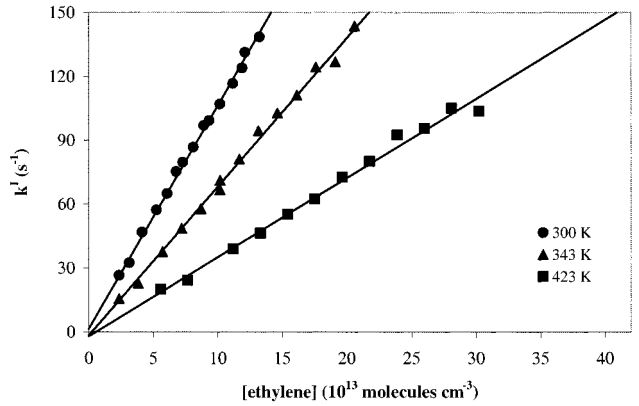

Figure 2. Plot of k^{I} versus ethylene concentration for the OH + ethylene reaction at 2 Torr and various temperatures.

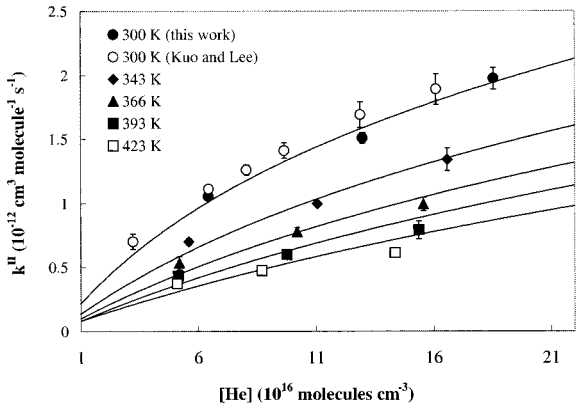

Figure 3. Plot of k^{II} versus [He] at five temperatures in the range 300−423 K for the OH + ethylene reaction. Uncertainties in the data represent 2 standard errors. The solid lines are the weighted least-squares fitting of the falloff behavior using eq 16 with $k_\infty = 1.96 \times 10^{-12}$ exp(438/T) cm^3 molecule^{-1} s^{-1} (ref 12).

Torr He, discharge flow − electron paramagnetic resonance). However, there are others who measured the rate constant for this reaction in He (e.g., Davis et al.,[24] Morris et al.,[25] and Pastrana and Carr[26]) who reported rate constants that are at least 30% larger than those reported here. The reasons for these discrepancies are not clear.

Falloff behavior of the effective bimolecular rate constant is observed for T = 300−423 K, as shown in Figure 3, and is consistent with the OH addition mechanism dominating under these conditions. The pressure and temperature dependence of reaction 1 is consistent with the following mechanism of the Lindemann−Hinshelwood type:

$$OH + C_2H_4 \rightarrow HOCH_2CH_2^* \quad (13)$$

$$HOCH_2CH_2^* \rightarrow OH + C_2H_4 \quad (14)$$

$$HOCH_2CH_2^* + M \rightarrow HOCH_2CH_2 + M^* \quad (15)$$

As the temperature is increased, the rate of dissociation (reaction 14) of the energized $HOCH_2CH_2$* complex relative to stabilization (reaction 15) increases, whereas the rate of stabilization increases with pressure.

According to Troe,[27−29] the falloff curve can be represented by

$$k^{II} = \left[\frac{k_0(T)[M]}{1 + (k_0(T)[M]/k_\infty(T))}\right] F_c^{(1+[\log(k_0(T)[M]/k_\infty(T))]^2)^{-1}} \quad (16)$$

TABLE 2: Termolecular Rate Constants Derived from Troe's Theory for the OH + Ethylene Reaction

T (K)	k_0 (10^{-29} cm^6 molecule^{-2} s^{-1})[a]
300	2.62 ± 0.25
343	1.58 ± 0.20
366	1.14 ± 0.13
393	0.91 ± 0.15
423	0.72 ± 0.20

[a] Uncertainties represent 2 standard errors.

where k_0 is the termolecular rate constant at the low-pressure limit, k_∞ is the effective bimolecular rate constant at the high-pressure limit, and F_c is the collision broadening factor. The collision-broadening factor corrects for the difference between an actual falloff curve and Lindemann−Hinschelwood behavior, which tends to overpredict rate constants in the region near the center of the falloff curve.[27−30] F_c decreases with increasing temperature, increasing number of vibrational modes, and increasing strength in the dissociating bond.[30] Given the limited pressure range in this study, both k_0 and k_∞ for reaction 1 cannot be calculated accurately. However, if the currently recommended value for k_∞ of 8.52×10^{-12} cm^3 molecule^{-1} s^{-1} and a value of 0.6 for F_c are used,[11,12] a weighted nonlinear least-squares fit of the data in Table 1 results in a value of $k_0 = (2.62 \pm 0.25) \times 10^{-29}$ cm^6 molecule^{-2} s^{-1} for the low-pressure limiting rate constant for reaction 1 at 300 K where the uncertainty represents two standard errors from the fit. This value is in good agreement with that obtained by Kuo and Lee in He and at 300 K [$k_0 = (2.74 \pm 0.04) \times 10^{-29}$ cm^6 molecule^{-2} s^{-1}].[10] However, it should be noted that in deriving k_0, Kuo and Lee assumed k_∞ to be $\sim 1.85 \times 10^{-12}$ exp(400/T) cm^3 molecule^{-1} s^{-1} and F_c = 0.7. A nonlinear least-squares fit of the rate constant data reported by Kuo and Lee in He using $k_\infty = 8.52 \times 10^{-12}$ cm^3 molecule^{-1} s^{-1} and a value of 0.6 for F_c results in a value of $k_0 = (3.02 \pm 0.05) \times 10^{-29}$ cm^6 molecule^{-2} s^{-1}, which is in reasonable agreement with the value obtained in this study.

These termolecular rate constants at 300 K for reaction 1 are smaller than the recommended value of $(1.0 \pm 0.6) \times 10^{-28}$ cm^6 molecule^{-2} s^{-1}.[11] They are also smaller than the k_0 values of $(5.9\ (+3.0)/(-1.0)) \times 10^{-29}$ and 5.5×10^{-29} cm^6 molecule^{-2} s^{-1}, which were determined from falloff fittings of measured rate constants in Ar at higher pressures by Klein et al.[31] (4−750 Torr) and by Zellner and Lorenz[32] (32−97 Torr), respectively. Because of these discrepancies, more measurements of rate constants at higher pressures are needed to fully characterize the falloff behavior for this reaction.[10]

Values of k_0 for reaction 1 derived from the measurements at other temperatures are listed in Table 2. These values were obtained by fitting the effective bimolecular rate constants measured at each temperature between 2 and 6 Torr to eq 16 and using recommended values for $F_c = 0.6$ and $k_\infty = 1.96 \times 10^{-12}$ exp(438/T) cm^3 molecule^{-1} s^{-1}.[11,12] Arrhenius parameters were determined by plotting the termolecular rate constants (k_0 values from Table 2) versus temperature, as shown in Figure 4. A weighted linear least-squares fit of the Arrhenius plot yielded the following expression for the temperature dependence of the rate constant for reaction 1 at the low-pressure limit, where the uncertainties represent two standard errors from the fit:

$$k_0 = (4.9 \pm 0.2) \times 10^{-31} \exp[(1210 \pm 130)/T] \text{ cm}^6 \text{ molecule}^{-2} \text{ s}^{-1} \quad (17)$$

This negative activation energy is similar to that obtained by Kuo and Lee (1560 ± 160 K) who derived k_0 for reaction 1 as

TABLE 3: OH + Isoprene Summary of Experimental Conditions and Results

T (K)	[He] (10^{16} molecules cm^{-3})	[Isoprene] (10^{12} molecules cm^{-3})	No. of expts	k^{II} (10^{-11} cm^3 molecule^{-1} s^{-1})[a]
300	5.76−6.08	0.38−1.65	45	10.99 ± 0.38
	12.13−13.45	0.39−1.65	40	11.22 ± 0.34
	18.86	0.42−1.63	12	11.10 ± 0.48
321	5.95	0.51−1.79	11	7.88 ± 0.50
	11.76	0.50−1.79	12	8.96 ± 0.30
	17.86	0.52−1.95	12	9.02 ± 0.34
343	5.57	0.49−2.45	11	5.93 ± 0.27
	11.68	0.44−2.00	13	6.62 ± 0.26
	17.02	0.81−2.33	12	7.51 ± 0.38
363	5.61	0.61−3.25	11	4.66 ± 0.19
	11.30	0.37−2.37	12	5.31 ± 0.28
	15.66	0.39−3.07	12	5.83 ± 0.24
383	4.96	0.76−3.54	12	3.98 ± 0.17
	9.90	0.54−2.82	11	4.66 ± 0.46
	15.17	0.62−3.31	12	4.98 ± 0.50
403	4.93	0.93−6.30	12	3.51 ± 0.14
	10.04	0.88−3.93	12	4.56 ± 0.21
	14.87	0.73−4.02	12	5.00 ± 0.28
423	5.55	1.45−5.91	12	3.34 ± 0.15
	9.06	1.09−4.97	12	3.85 ± 0.33
	14.74	0.61−4.26	12	4.62 ± 0.20

Flow velocity	10.1−14.7 m s^{-1}
Carrier gas	He w/10% O_2
OH concentration	$<3 \times 10^{11}$ cm^{-3}
O_2 concentration	$(2-8) \times 10^{15}$ cm^{-3}
Stoichiometric ratio	~3−30
Diffusion coefficient	OH in He, $0.145T^{3/2}/P$ (<5% correction)
First-order wall removal rate	<24 s^{-1} (in presence of 10% O_2)

[a] Uncertainties represent 2 standard errors.

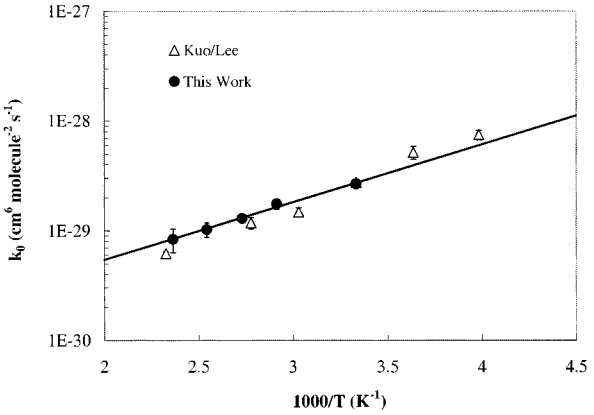

Figure 4. Arrhenius plot of the termolecular rate constants for the OH + ethylene reaction derived from eq 16 with $k_\infty = 1.96 \times 10^{-12}$ exp(438/T) cm^3 molecule^{-1} s^{-1} (ref 12). Solid line is the weighted least-squares fitting of the k_0 values from this work. Uncertainties represent 2 standard errors.

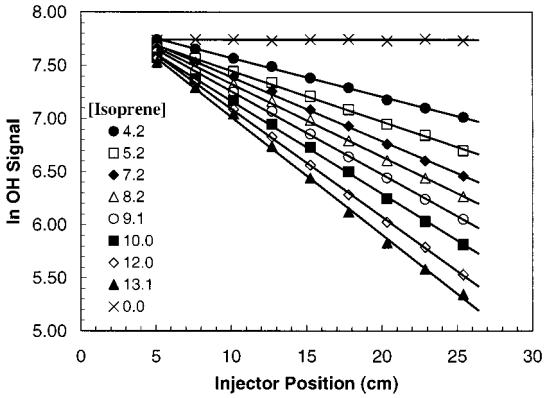

Figure 5. Sample pseudo-first-order decays of OH for the OH + isoprene reaction at 2 Torr and 300 K (isoprene concentrations in 10^{11} cm^{-3}).

a function of temperature using $F_c = 0.7$ and a value for k_∞ of ~1.85×10^{-12} exp(400/T) cm^3 molecule^{-1} s^{-1}.[10] Fitting the data reported by Kuo and Lee in He to eq 16 using $F_c = 0.6$ and $k_\infty = 1.96 \times 10^{-12}$ exp(438/T) cm^3 molecule^{-1} s^{-1} results in a negative activation energy of (1530 ± 160) K for this reaction.

The termolecular rate constants obtained in this study were also fitted to the equation

$$k_0 = k_0^{300}(T/300)^{-n} \qquad (18)$$

with $n = 3.5 \pm 0.2$ obtained for k_0. This value is similar to that obtained by Kuo and Lee ($n = 4.8$). These values of n are larger than the recommended n value of 0.8 ± 2.0 that is based on theoretical considerations.[11]

OH + Isoprene. Table 3 summarizes the experimental conditions and results for reaction 8. Typical decays of OH are shown in Figure 5, and typical plots of k^{I}_{obsd} at 2 Torr and 300, 343, and 403 K versus isoprene concentration appear in Figure 6. A weighted linear least-squares fit of the 300 K plot yields a value of $k^{II}_{300} = (1.10 \pm 0.04) \times 10^{-10}$ cm^3 molecule^{-1} s^{-1} for the effective bimolecular rate constant at 2 Torr. The reported uncertainty is two standard errors from the precision of the weighted least-squares regression. The rate constant at 300 K was independent of the fraction of isoprene in the reservoir mixture, suggesting that heterogeneous loss of isoprene on the uncoated glass wall of the reservoir was minimal. As already described, heterogeneous effects due to the presence of isoprene in the flow reactor were minimized by the addition of O_2 to the system, resulting in first-order wall removal rates of OH (reflected by the intercepts of the second-order plots of k^{I} versus isoprene concentration) that were always <24 s^{-1}, but typically

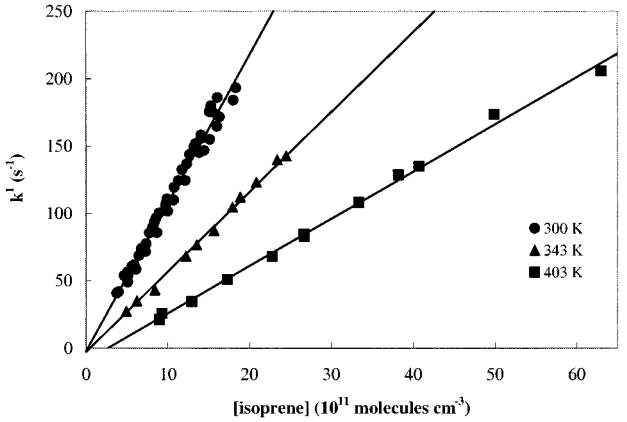

Figure 6. Plot of k^I versus isoprene concentration for the OH + isoprene reaction at 2 Torr and various temperatures.

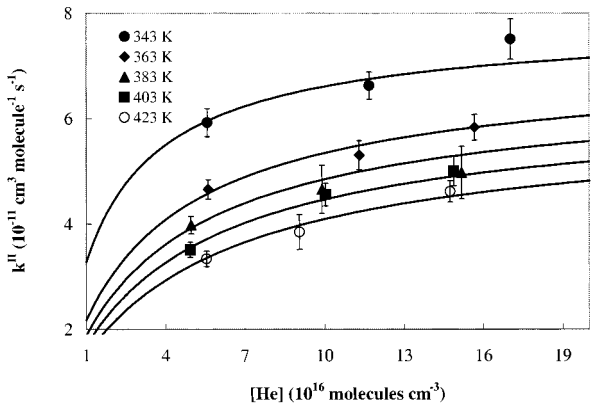

Figure 7. Plot of k^{II} versus [He] at five temperatures in the range 343−423 K for the OH + isoprene reaction. Uncertainties in the data represent 2 standard errors. The solid lines are the weighted least-squares fitting of the falloff behavior using eq 16 and assuming $k_\infty = 2.54 \times 10^{-11}$ exp(410/T) cm^3 $molecule^{-1}$ s^{-1} (ref 12).

<10 s^{-1}. These intercepts were similar to the first-order wall-loss rates of OH measured in the absence of isoprene (<10 s^{-1}), suggesting that in the presence of O_2, the isoprene-catalyzed loss of OH on the reactor walls was not interfering with the rate constant measurements. One might expect the contribution of the isoprene-catalyzed wall-loss of OH to decrease as the temperature increases due to the decreased partitioning of isoprene to the walls of the flow tube. However, the intercepts in the second-order plots did not show any correlation with temperature, again suggesting that the presence of O_2 inhibits the isoprene-catalyzed heterogeneous loss of OH on the reactor walls.

Unlike reaction 1, reaction 8 does not exhibit a pressure dependence at room temperature between 2 and 6 Torr [(1.10 ± 0.04), (1.12 ± 0.03), and (1.11 ± 0.05) × 10^{-10} cm^3 $molecule^{-1}$ s^{-1}, respectively]. Although the lack of a pressure dependence may suggest that an H atom abstraction mechanism may be occurring at low pressures, the observed rate constant for reaction 8 decreases with increasing temperature (Table 3). These measurements are the first reported of the pressure and temperature dependence of this reaction in this pressure range, and they suggest that the reaction mechanism is dominated by OH addition rather than by H atom abstraction even at the low pressures and high temperatures of these experiments.

The results at room temperature agree well with the rate constant of (9.26 ± 1.5) × 10^{-11} cm^3 $molecule^{-1}$ s^{-1} measured by Kleindienst et al.[14] in 50 Torr of argon using a flash photolysis−resonance fluorescence technique. The measurements in this study also agree well with measurements obtained from relative rate studies in air at 1 atm, as reviewed by Atkinson,[15] resulting in a recommended rate constant of 1.01 × 10^{-10} cm^3 $molecule^{-1}$ s^{-1}. The agreement between the rate constants measured at low pressures (2, 4, and 6 Torr) as reported here with those at higher pressures suggests that at room temperature, reaction 8 has reached its high-pressure limit at 2 Torr. This result indicates that the larger number of available vibrational degrees of freedom allows the hydroxyalkyl radical produced in reaction 8 to easily distribute the excess energy resulting from the electrophilic addition of OH to a double bond in isoprene, and stabilize the adduct with a minimal number of third-body collisions. The nonpressure dependence of reaction 8 at room temperature is similar to the rate constants of the reactions of OH with $\geq C_4$ alkenes[12] and results obtained for the Cl + isoprene addition reaction.[20] However, these results are in contrast to recent direct measurements of the rate constant for reaction 8 in N_2, N_2/O_2, and He by Campuzano-Jost et al.

TABLE 4: Termolecular Rate Constants Derived from Troe's Theory for the OH + Isoprene Reaction

T (K)	k_0 (10^{-27} cm^6 $molecule^{-2}$ s^{-1})[a]
343	10.50 ± 1.57
363	6.71 ± 0.36
383	5.36 ± 0.34
403	4.53 ± 0.17
423	3.74 ± 0.15

[a] Uncertainties represent 2 standard errors.

using pulsed laser photolysis−pulsed laser-induced fluorescence techniques.[16] These authors report a room-temperature rate constant of (8.56 ± 0.26) × 10^{-11} cm^3 $molecule^{-1}$ s^{-1} that is independent of pressure or bath gas composition between 60 and 600 Torr.

Falloff behavior for reaction 8 is observed for $P = 2-6$ Torr at temperatures of 343 K and higher, as shown in Figure 7. This behavior is consistent with a Lindemann−Hinshelwood mechanism:

$$\text{OH} + \text{isoprene} \rightarrow \text{HO} - \text{isoprene}^* \quad (19)$$

$$\text{HO} - \text{isoprene}^* \rightarrow \text{OH} + \text{isoprene} \quad (20)$$

$$\text{HO} - \text{isoprene}^* + \text{M} \rightarrow \text{HO} - \text{isoprene} + \text{M}^* \quad (21)$$

However, unlike the $HOCH_2CH_2$* complex, the rate of dissociation of the HO−isoprene* complex (reaction 20) does not compete with the rate of stabilization (reaction 21) until the temperature is increased to >343 K. This result is likely due to the ability of the complex to distribute energy into many vibrational modes, reducing the energy in the critical CO vibration. Ab initio calculations on the HO−isoprene adduct indicate that the vibrational modes are highly coupled with each other.[33]

Because of the limited pressure range in this study, both k_0 and k_∞ at $T = 343-423$ K for reaction 8 cannot be determined accurately. However, using the recommended $F_c = 0.6$ and $k_\infty = 2.54 \times 10^{-11}$ exp(410/T) cm^3 $molecule^{-1}$ s^{-1},[11,12] a weighted nonlinear least-squares fit of the k^{II} data at $T = 363-423$ K according to eq 16 would yield the k_0 values listed in Table 4. The data at 343 K are more consistent with $F_c = 0.7$, which is not surprising because collisional broadening decreases with increasing temperature.[30]

Arrhenius parameters for reaction 8 were determined by plotting the derived k_0 values versus temperature, as shown in

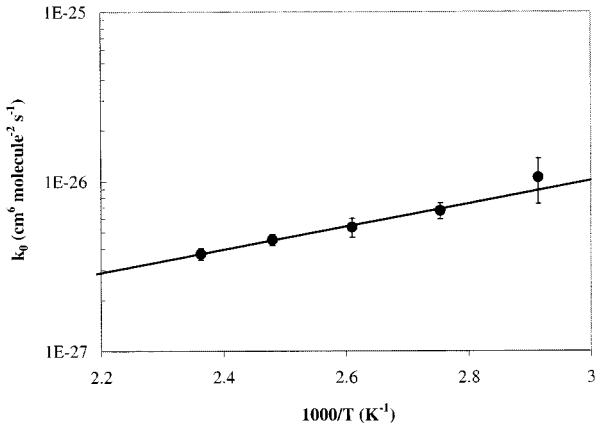

Figure 8. Arrhenius plot of the termolecular rate constants for the OH + isoprene reaction derived from eq 16 with $k_\infty = 2.54 \times 10^{-11}$ exp(410/T) cm^3 molecule^{-1} s^{-1} (ref 12). Uncertainties in the data represent 2 standard errors. The solid line is the weighted linear least-squares fitting of the data.

Figure 8. A weighted linear least-squares fit yields the following equation, with the uncertainties representing two standard errors:

$$k_0 = (9.3 \pm 5.4) \times 10^{-29} \exp[(1560 \pm 230)/T] \text{ cm}^6 \text{ molecule}^{-2} \text{ s}^{-1} \quad (22)$$

The negative activation energy for the low-pressure limiting rate constant obtained is similar to that for the OH + ethylene reaction and is consistent with an OH addition mechanism.

Conclusions

Measurements of the rate constant for the OH + ethylene reaction at 300 K in He with 10% O_2 are in good agreement with previous measurements under similar conditions. However, measurements of the pressure dependence of these rate constants resulted in a smaller termolecular rate constant at the low-pressure limit than current recommendations. A strong temperature dependence is observed for the termolecular rate constant at the low-pressure limit. Although the magnitude of the negative activation energy observed is larger than the recommended value, it is in good agreement with that reported by Kuo and Lee[10] in He under similar conditions.

Unlike the OH + ethylene reaction, the rate constant for the OH + isoprene reaction is not pressure dependent at room temperature. However, at temperatures >343 K, the OH + isoprene reaction begins to show a dependence on pressure. Although the lack of a pressure dependence at room temperature may suggest that an abstraction mechanism may be occurring under these conditions, the observed temperature dependence suggests that the reaction is dominated by an addition mechanism even at the lowest pressures and highest temperatures of these experiments. The data for isoprene are the first set of direct measurements of the temperature and pressure dependence for this pressure range.

The measured rate constants at 2, 4, and 6 Torr of He with 10% O_2 and 300 K are in good agreement with direct measurements of the OH + isoprene rate constant at 50 Torr of Ar,[14] and those measured at 1 atm by relative rate studies.[15] However, the room-temperature results in this study are not in good agreement with recent direct measurements of the rate constant between 60 and 600 Torr of He, N_2, and N_2/O_2 by Campuzano-Jost et al.,[16] although the latter results are in good agreement with the results of Kleindienst et al.[14] The reasons for this difference are unclear. Further direct measurements of the rate constant for the OH + isoprene reaction under a wide range of conditions and using a variety of techniques are needed to resolve this discrepancy.

Termolecular rate constants at the low-pressure limit for the OH + isoprene reaction derived from Troe's expression appear to be highly temperature dependent. The activation energy of the rate constant at the low-pressure limit is similar to that for ethylene observed in this study. These measurements of the low-pressure limiting rate constants are also in good agreement with theoretical calculations based on simplified RRKM theory and ab initio calculations of the HO−isoprene adduct.[33]

Because of the limited pressure range under study, further studies covering a broader pressure range and over an extended temperature range are needed to fully characterize the falloff behavior of both the OH + ethylene and OH + isoprene reactions. Future experiments will expand the pressure range used in this study using turbulent flow techniques and will examine the kinetics of some of the subsequent steps in the oxidation mechanism.

Acknowledgment. This work is supported by the National Science Foundation, grant ATM-9622712. Acknowledgment is also made to the donors of the Petroleum Research Fund, administered by the American Chemical Society, for support of this research (grant PRF 33643-G6). We also thank P. Campuzano-Jost and Professor A. Hynes for a preprint of ref 16, and the reviewers of this manuscript for their critical and constructive comments.

References and Notes

(1) Seinfeld, J. H.; Pandis, S. N. *Atmospheric Chemistry and Physics: From Air Pollution to Climate Change*; John Wiley: New York, 1998; pp 264−313.

(2) Orlando, J. J.; Tyndall, G. S.; Bilde, M.; Ferronato, C.; Wallington, T. J.; Vereecken, L.; Peeters, J. *J. Phys. Chem. A* **1998**, *102*, 8116.

(3) Lamb, B.; Guenter, A.; Gay, D.; Westburg, H. *Atmos. Environ.* **1987**, *21*, 1695.

(4) Lloyd, A. C.; Atkinson, R.; Lurmann, F. W.; Nitta, B. *Atmos. Environ.* **1983**, *17*, 1931.

(5) Atkinson, R.; Aschmann, S. M.; Tuazon, E. C.; Arey, J.; Zielinska, B. *Int. J. Chem. Kinet.* **1989**, *21*, 593.

(6) Paulson, S. E.; Flagan, R. C.; Seinfeld, J. H. *Int. J. Chem. Kinet.* **1992**, *24*, 79.

(7) Carter, W. P. L.; Atkinson, R. *Int. J. Chem. Kinet.* **1996**, *28*, 497.

(8) Sawada, S.; Totsuka, T. *Atmos. Environ.* **1986**, *20*, 821.

(9) Singh, H. B.; Zimmerman, P. R. Atmospheric distribution and sources of nonmethane hydrocarbons. In *Gaseous Pollutants: Characterization and Cycling*; Nriagu, J. O., Ed.; John Wiley: New York, 1992; pp 177−235.

(10) Kuo, C.-H.; Lee, Y.-P. *J. Phys. Chem.* **1991**, *95*, 1253.

(11) DeMore, W. B.; Sander, S. P.; Golden, D. M.; Hampson, R. F.; Kurylo, M. J.; Howard, C. J.; Ravishankara, A. R.; Kolb, C. E.; Molina, M. J. *Chemical Kinetics and Photochemical Data for Use in Stratospheric Modeling*; NASA JPL Publ. No. 97-4, Jet Propulsion Laboratory: Pasadena, CA, 1997.

(12) Atkinson, R. *J. Phys. Chem. Ref. Data* **1997**, *26*, *n6*, 1329.

(13) Stevens, P.; L'Esperance, D.; Chuong, B.; Martin, G. *Int. J. Chem. Kinet.* **1999**, *31*, 637.

(14) Kleindienst, T. E.; Harris, G. W.; Pitts, J. N., Jr. *Environ. Sci. Technol*. **1982**, *16*, 844.

(15) Atkinson, R. *J. Phys. Chem. Ref. Data*. **1989**, *18*, Monograph 1, 881.

(16) Campuzano-Jost, P.; Williams, M. B.; D'Ottone, L.; Hynes, A. J. *Geophys. Res. Lett.* **2000**, *27*, 693.

(17) McKeen, S. A.; Mount, G.; Eisele, F.; Williams, E.; Harder, J.; Goldan, P.; Kuster, W.; Liu, S. C.; Baumann, K.; Tanner, D.; Fried, A.; Sewell, S.; Cantrell, C.; Shetter, R. *J. Geophys. Res*. **1997**, *102*, 6467.

(18) Loewenstein, L. M.; Anderson, J. G. *J. Phys. Chem.* **1984**, *88*, 6227.

(19) Stutz, J. Ezell, M. J.; Ezell, A. A.; Finlayson-Pitts, B. J. *J. Phys. Chem. A* **1998**, *102*, 8510.

(20) Bedjanian, Y.; Laverdet, G.; LeBras, G. *J. Phys. Chem. A* **1998**, *102*, 953.

(21) Howard, C. J. *J. Phys. Chem.* **1979**, *83*, 3.

(22) Howard, C. J. *J. Chem. Phys.* **1976**, *65*, 4771.

(23) Bradley, J. N.; Hack, W.; Hoyermann, K.; Wagner, H. G. *J. Chem. Soc., Faraday Trans.* **1973**, *69*, 1889.
(24) Davis, D. D.; Fischer, S.; Schiff, R.; Watson, R. T.; Bollinger, W. *J. Chem. Phys.* **1975**, *63*, 1707.
(25) Morris, E. D., Jr.; Stedman, D. H.; Niki, H. *J. Am. Chem. Soc.* **1971**, *93*, 3570.
(26) Pastrana, A. V.; Carr, R. W., Jr. *J. Phys. Chem.* **1975**, *79*, 765.
(27) Troe, J. *J. Chem. Phys.* **1977**, *66*, 4745.
(28) Troe, J. *J. Chem. Phys.* **1977**, *66*, 4758.
(29) Troe, J. *J. Phys. Chem.* **1979**, *83*, 114.
(30) Donahue, N. M.; Dubey, M. K.; Anderson, J. G. *J. Geophys. Res.* **1997**, *102*, 6159.
(31) Klein, T.; Barnes, I.; Becker, K. H.; Fink, E. H.; Zabel, F. *J. Phys. Chem.* **1984**, *88*, 5020.
(32) Zellner, R. Lorenz, K. *J. Phys. Chem.* **1984**, *88*, 984.
(33) Stevens, P. S.; Seymour, E.; Li, Z. submitted for publication in *J. Phys. Chem. A.*